

Exciton and carrier dynamics in ZnTe-Zn_{1-x}Mg_xTe core-shell nanowiresM. Szymura,¹ Ł. Kłopotowski,^{1,*} A. A. Mitioglu,^{2,3} P. Wojnar,¹ G. Karczewski,¹ T. Wojtowicz,¹ D. K. Maude,² P. Plochocka,² and J. Kossut¹¹*Institute of Physics, Polish Academy of Sciences, Al. Lotników 32/46, 02-668 Warsaw, Poland*²*LNCMI, CNRS-UJF-UPS-INSA, F-38042 Grenoble and F-31400 Toulouse, France*³*Institute of Applied Physics, Academiei Str. 5, Chisinau, MD-2028, Republic of Moldova*

(Received 4 November 2015; revised manuscript received 10 March 2016; published 25 April 2016)

We employ time-resolved photoluminescence combined with scanning electron microscopy and modeling to evaluate the lifetimes of excitons and free carriers in core-shell ZnTe-Zn_{1-x}Mg_xTe nanowires. We find that electron tunneling through the shell to the surface controls the decay dynamics. The photoluminescence of single nanowires reveals contributions from an electron-hole plasma. The analysis of its temporal behavior allows one to extract the carrier and exciton lifetimes and monitor the cooling dynamics. In particular, we demonstrate that most of the electrons tunnel out before they cool down or bind into excitons. A semiclassical model allows us to extract the contributions of tunneling and recombination to the photoluminescence decay. We find that the recombination time shortens with increasing temperature as a result of an activation of a phonon-assisted nonradiative process.

DOI: [10.1103/PhysRevB.93.155429](https://doi.org/10.1103/PhysRevB.93.155429)**I. INTRODUCTION**

The bottom-up assembly of semiconductor nanowires (NWs) offers a possibility of combining materials, which would be incompatible in planar growth due to, e.g., excessive lattice mismatch. One-dimensional (1D) geometry of NWs allows one to embed either radial or axial nanostructures. These properties result in a plethora of devices, in which the NWs could be used. These include light sources such as lasers [1,2], light emitting diodes [3–5], components for multicolor displays [6], single photon emitters [7,8], sources of entangled photon pairs [9,10], and photodetectors [11–13]. Moreover, their large surface-to-volume ratio offers a possibility of applications as sensors for single molecule detection [14] and solar cells [15,16]. In order to fulfill this application potential, detailed knowledge of carrier dynamics is essential. It was shown that carrier and photoluminescence (PL) lifetimes in NWs are limited by surface recombination. Fabrication of a shell around the NW core results in an increase of the carrier lifetime by several orders of magnitude [17–23]. Passivation of surface states led to the observation of carrier lifetimes comparable [17,19,21] to or even longer [23] than the values intrinsic to high quality planar structures. Although the presence of the shell clearly enhances both the PL intensity and lifetime, the microscopic mechanism underlying this effect is not clear. In fact, it was shown that passivated NWs still exhibit surface-limited lifetimes related to the states at the core-shell interface [18].

Zinc telluride NWs share many of the potential device applications of their III-V counterparts. They exhibit a high photosensitivity [24,25], can be grown by molecular beam epitaxy using gold droplets as catalysts [26], and reveal an efficient excitonic photoluminescence [22,27]. CdTe quantum dots embedded into these NWs emit single photons on demand [28]. These functionalities can be extended by doping with transition metal ions and such semimagnetic NWs reveal

pronounced magneto-optical effects [29–31]. However, little is known about the dynamical properties of electrons, holes, and excitons in these nanostructures.

In this report, we evaluate carrier and exciton lifetimes from studies of the PL decay dynamics of ensembles and individual core-shell ZnTe-Zn_{1-x}Mg_xTe NWs. We show that the PL decay time crucially depends on the shell thickness, which controls the tunnel escape rate from the core to the surface states. A simple semiclassical model allows us to reproduce the observed nonexponential decay dynamics and extract the exciton recombination times. The decay time is defined as $\tau_d^{-1} = \tau_r^{-1} + \tau_t^{-1}$ where the radiative lifetime $\tau_r \simeq 340$ ps is independent of shell thickness and the tunneling time $\tau_t \simeq 10$ –30 ps for shell thicknesses in the range 12–16 nm. We show that, as the temperature is increased, the decays accelerate as a result of activation of a phonon-assisted nonradiative process. Furthermore, time-resolved studies of single NWs reveal that the exciton PL coincides temporally with the recombination from an electron-hole plasma. Many-body interactions give rise to a band gap renormalization resulting in a broad time-integrated spectrum. Decay analysis at various photon energies allows us to evaluate the lifetime of excitons and electron-hole plasma and extract its cooling dynamics.

II. SAMPLES AND EXPERIMENT

Core-shell ZnTe-Zn_{1-x}Mg_xTe NWs are grown in a molecular beam epitaxy chamber by applying a vapor-liquid-solid (VLS) mechanism [32]. First, a 1-nm thick gold layer is deposited on a (111)-oriented Si substrate. The layer is then heated to above 500°C to form droplets of gold/Si eutectic about 10 nm in diameter. The droplets act as catalysts for the VLS axial growth of the core, which takes place at 370°C–380°C. To grow the shell in the radial direction, the temperature is lowered to 300°C–320°C.

We investigated six different samples. Five of them form a series, in which the core is grown for 25 min, while the Zn_{1-x}Mg_xTe shell is grown for 0, 2, 4, 6, and 8 min. The Mg molar fraction $x \approx 0.35$ is determined from energy dispersive

*lukasz.klopotowski@ifpan.edu.pl

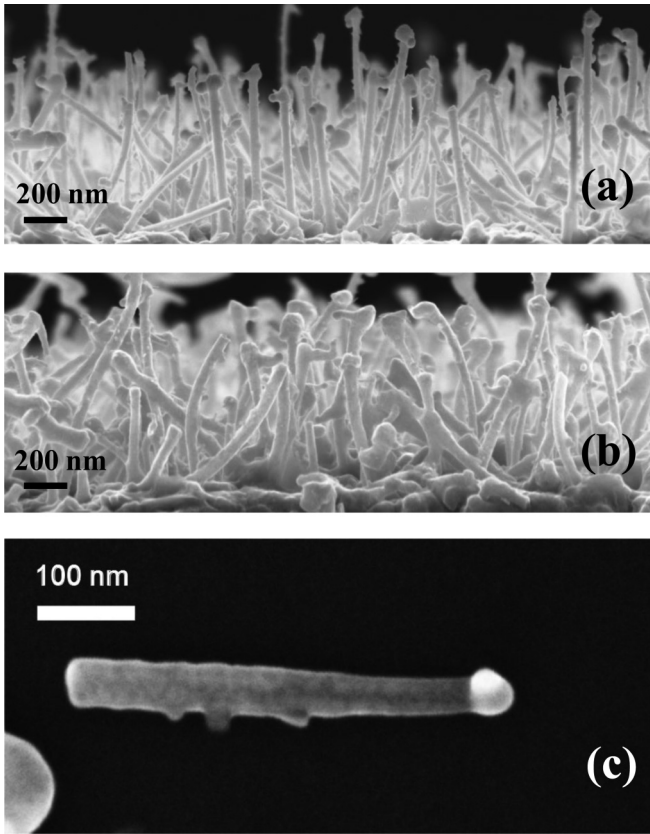


FIG. 1. SEM images of ensembles of as-grown core-shell ZnTe-Zn_{1-x}Mg_xTe NWs with $R = 9.5$ nm core radius and (a) $L = 8$ nm (b) and $L = 16$ nm shell thickness. (c) SEM image of a single NW with 16-nm shell thickness removed from the ensemble by sonication.

x-ray diffraction [33]. Additionally, for the studies of single NWs, another sample is grown, with the ZnTe core grown for 70 min, while the Zn_{1-x}Mg_xTe shell is grown for 9 min with $x \approx 0.3$. In the following, we label the samples from the series with their shell thicknesses and refer to the additional sample as S2.

The morphology of the NWs is examined by scanning electron microscope (SEM). Figures 1(a) and 1(b) show SEM images of ensembles of NWs from the 4-min and 8-min samples, respectively. It is seen that the NWs grow in arbitrary directions. This is due to an amorphous structure of the natural SiO₂ layer on top of which the gold catalysts are formed. The NW length reaches 1 μ m and the diameter clearly depends on the shell growth time. To determine the core radius and shell thicknesses (R and L , respectively), we perform a survey of about 100 individual NWs from each of the samples. For the ZnTe core-only NWs, we find that the average $R = 9.5 \pm 2.5$ nm. Since the exciton Bohr radius in ZnTe is about 5 nm [34], the confinement effects can be neglected and we can treat the NWs as a bulk material, albeit with a characteristic 1D geometry. The average L values for the 2-, 4-, 6-, and 8-min samples from the series are 3-, 8-, 12-, and 16-nm, respectively. In the case of the S2 sample, the average thickness of the core-shell NWs, $2R + 2L$ is 74 nm. The average NW density is about $25 \mu\text{m}^{-2}$.

The continuous wave (cw) photoluminescence (PL) from the ensemble of NWs is measured in a closed-cycle helium cryostat. The cw PL is excited at 473 nm by a solid state laser and detected with a monochromator with a resolution of 0.2 nm and a CCD camera. For time-resolved photoluminescence (TRPL) measurements the samples are mounted on a cold-finger cryostat and excited at 505 nm by the frequency doubled output of an optical parametric oscillator pumped with a pulsed Ti:sapphire femtosecond laser with a repetition rate of 80 MHz. Temporal pulse width is about 300 fs. The laser beam is focused onto a $\sim 2\text{-}\mu\text{m}$ spot with a microscope objective corresponding to excitation of about 50 NWs. The emitted light is collected with the same objective and detected by a streak camera synchronized with the excitation source. A single photon counting technique is used and the temporal resolution of the setup is ~ 7 ps. Both the cw and TRPL measurements are carried out in a temperature range between 5 and 100 K. In order to investigate the PL from a single NW, we sonicate an as-grown sample in isopropanol to remove the NWs into a solution, which is then drop cast onto a silicon wafer. Figure 1(c) shows a typical SEM image of a single NW from the sample with an average shell thickness of 16 nm. The image shows that some of the NWs exhibit a tapered shape. In such a case, L is determined as an average between the base and top widths.

III. ENSEMBLE PHOTOLUMINESCENCE

We start with showing the influence of the shell thickness on the PL energy and intensity. Figure 2(a) shows normalized PL spectra from ensembles of NWs from the sample series. With increasing the shell thickness, a redshift of the PL maximum is observed: from 2330 meV for $L = 3$ nm to 2280 meV for $L = 16$ nm. This redshift is a manifestation of the effect of the tensile strain exerted by the Zn_{1-x}Mg_xTe shell on the NW core, resulting in a decrease of the ZnTe band gap [33]. Moreover, with increasing L the PL intensity strongly increases. In particular, the PL intensity for NWs with $L = 16$ nm is more than two orders of magnitude larger than for NWs with $L = 3$ nm while ZnTe core-only NWs do not exhibit any near band gap PL [22]. Such a strong increase of the PL intensity was also observed for GaAs NWs where the surface states were passivated with an AlGaAs shell [35,36].

Figure 2(b) shows normalized TRPL traces recorded at 5 K for the ensembles of NWs with different L . The excitation fluence for all the traces is $100 \mu\text{J}/\text{cm}^2$. This relatively high excitation density is necessary to observe the PL signal from the samples with thinnest shells and weakest PL intensities. The transient intensities are obtained by integrating the entire PL signal, i.e., within an energy window of 140 meV. It is clear that the PL lifetime increases with L . However, a non-exponential decay hinders the evaluation of the characteristic decay time. For $L = 16$ nm sample, the PL decreases by a factor of 100 about 440 ps after reaching the maximum. On the other hand, the temporal width of the TRPL trace for the two samples with thinnest shells are resolution limited.

Figure 3(a) shows the normalized PL decays measured for temperatures between 5 and 100 K for the ensemble of NWs with $L = 16$ nm. It is seen that the decay rate accelerates with temperature. At 100 K, the PL intensity decreases by a factor of

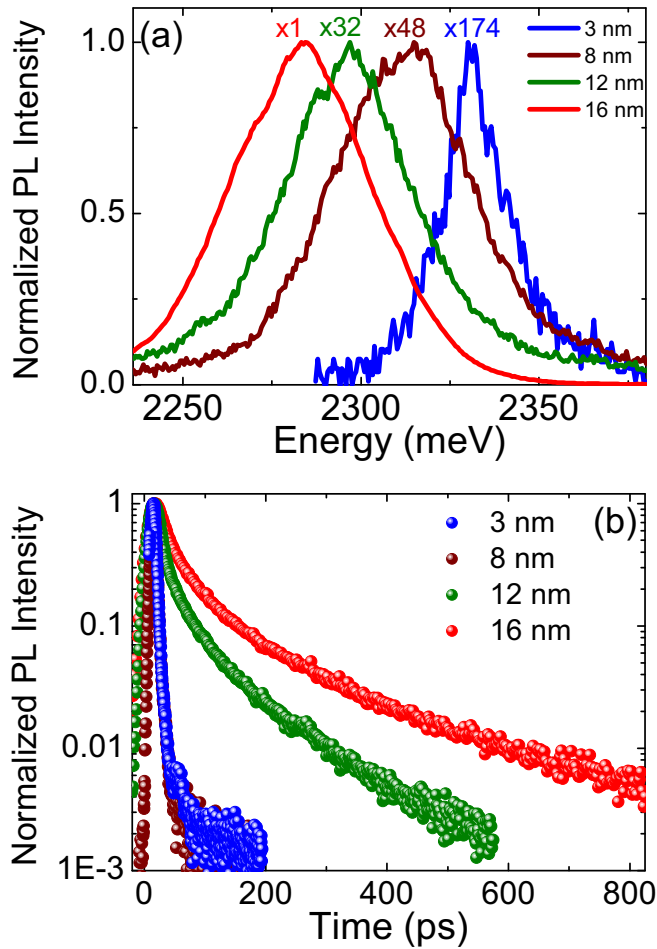


FIG. 2. (a) Normalized PL spectra collected at 5 K from ensembles of NWs with various shell thickness ranging from 3 nm to 16 nm. Normalization factors are given on top of each spectrum. (b) Normalized time-resolved PL traces of the ensembles of NWs with different shell thicknesses recorded at 5 K.

100 after a delay of only 105 ps. Also, the time-integrated PL intensity decreases with increasing temperature (not shown). To get an insight into the mechanisms responsible for the observed thermal quenching, we analyze the temperature dependence of cw PL. In Fig. 3(b) we plot the relative PL intensity $I(0)/I(T) - 1$ as a function of inverse temperature. $I(T)$ is the temperature-dependent PL intensity, $I(0)$ is its value extrapolated to 0 K. In order to obtain the activation energies for the thermal quenching, we fit the data in Fig. 3(b) with

$$\frac{I(0)}{I(T)} - 1 = C_1 \exp(-E_1/k_B T) + C_2 \exp(-E_2/k_B T), \quad (1)$$

where k_B is the Boltzmann constant, E_1 and E_2 are the activation energies for two different quenching processes, C_1 and C_2 are the corresponding radiative to nonradiative recombination efficiency ratios. From the fit, we find $E_1 \approx 1.3$ meV and $E_2 = 27.9$ meV. The evaluation of E_1 is subject to significant errors since its influence is seen only in the narrow temperature range up to about 20 K. Tentatively, we ascribe the quenching process at low temperatures to a thermal escape of electrons from NW cores to the surface states.

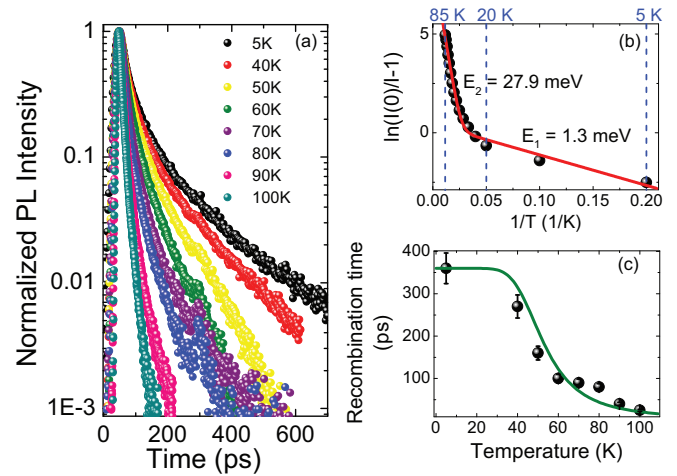


FIG. 3. (a) Normalized time-resolved PL decays as a function of temperature for ensemble of NWs with $L = 16$ nm. (b) (Points) Measured, normalized cw PL intensity as a function of inverse temperature. (Line) Fitted two-step thermal activation model [see Eq. (1)]. E_1 and E_2 are the fitted activation energies. (c) (Points) Temperature dependence of the recombination time evaluated from (a). (Line) Calculated temperature dependence of the recombination time taking into account thermal activation of a nonradiative process. See text for details.

Below, we show arguments supporting this hypothesis. E_2 is close to the bulk ZnTe longitudinal optical (LO) phonon energy, 26.1 meV [37]. Therefore, we interpret E_2 as an activation of nonradiative recombination by the exciton-LO phonon interaction, dominant at high temperatures.

We now turn to the interpretation of the presented experimental data and elucidation of the processes controlling the PL dynamics. The results presented above, i.e., shortening of the PL decay time and ultimately vanishing of the PL signal with decreasing shell thickness and shortening of the PL decay time with increasing temperature could be caused by a band-bending effect. It results from pinning of the Fermi level at the surface states and leads to a depletion layer inside the NW core [18,38]. In such a case, the nonradiative recombination is driven by recombination at the surface or an interface and its rate is given by $\tau_{\text{nr}}^{-1} = 4S/d$, where d is the NW diameter and S denotes surface recombination velocity. The effect of band bending is slowing down of surface recombination as the built-in electric field pushes the carriers away from the edge. Phenomenologically, this effect can be accounted for by taking $S = S_0 \exp(-\phi/(k_B T))$, where S_0 is the flatband value and ϕ is the band-bending parameter [39–41]. The presence of a large density of carriers, e.g., created by an ultrashort laser pulse, partially screens out the built-in field and results, on one hand, in a blueshift of the PL, and on the other in an acceleration of the PL decay due to enhanced surface recombination [42]. In order to check whether band bending could be responsible for the quenching of the PL and accelerating its decay for the NWs with thin shells, we investigated the PL dynamics in a range of excitation fluences between 60 and 270 $\mu\text{J}/\text{cm}^2$. We found that the decay time is insensitive to the excitation fluence in this range and that there is no shift of the PL peak within 0.1 of its linewidth. For this range of fluence, the PL

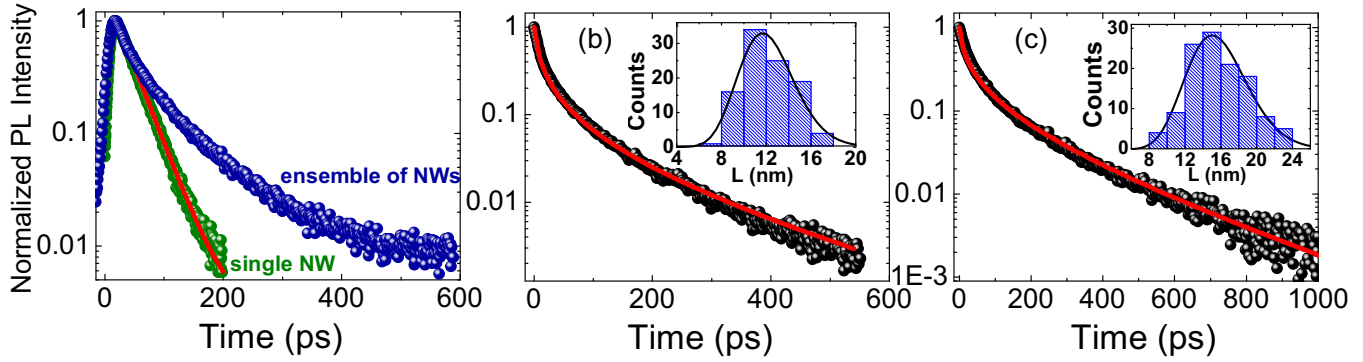


FIG. 4. (a) Comparison between ensemble (blue) and single NW (green) time-resolved PL traces. Ensemble PL exhibits a nonexponential temporal decay. The decay from a single NW is monoexponential. (b) and (c) (Points) Time-resolved PL trace from an ensemble of NWs with $L = 12$ nm and $L = 16$ nm, respectively. (Lines) Fitted PL decay (see text for details). The insets show the respective distributions of the shell thicknesses L with a fitted Gamma distribution function.

emission intensity is not saturated, which indicates that the density of photocreated carriers continues to increase, with increasing fluence. We therefore conclude that band bending has a negligible influence on the PL properties of these ZnTe NWs for the range of fluence investigated.

As mentioned above, for an ensemble of NWs a nonexponential PL decay is observed, precluding the determination of a PL decay time. In order to understand the PL properties of the ensemble of NWs and to assess the origin of the effects presented above, we compare the ensemble PL decay with that of a single NW. In Fig. 4(a), we show the normalized PL decays for an NW ensemble and a single NW both from the S2 sample. The PL decay from an individual NW is clearly monoexponential and the decay time for this particular NW is $\tau_d = 31 \pm 1$ ps. We have investigated several individual NWs and the decay is always monoexponential, with decay times in the range $\simeq 5$ –31 ps. We therefore conclude that the nonexponential behavior results from the fact that in the measurements on the NW ensemble, we excite and collect the PL signal from about 50 NWs. In such a case, the nonexponential PL decay results from a superposition of different monoexponential decays from the individual NWs [43]. In the following, we apply a simple model to show that the variation of the PL decay time between the NWs originates from different tunnel escape rates from the core to the surface states.

We assume that the PL decay contains a contribution from the recombination, represented by time τ_r and independent of the shell thickness, and from carrier tunneling out of the NW core with time τ_t strongly dependent on L . Thus, the decay time is defined as $\tau_d^{-1} = \tau_r^{-1} + \tau_t^{-1}$. Since the conduction band offset is about 20% of the total difference between ZnTe core and $\text{Zn}_{1-x}\text{Mg}_x\text{Te}$ shell band gaps [44,45], the barrier height for electrons is four times smaller than for the holes. Moreover, the electrons are roughly six times lighter than holes. As a result, the expected tunneling times for the holes are orders of magnitude longer than for electrons and in the following we neglect the influence of the holes. We calculate τ_t within a quasiclassical approach in which $\tau_t = \tau_s T^{-1}$, where τ_s is an average time for an electron in the core to reach the core-shell interface and T is the textbook transmission coefficient for tunneling through a rectangular

barrier. $T = T(E_k, V, L)$, where E_k is the average electron kinetic energy and V is the barrier height. To calculate τ_s , we take the average distance from the electron to the core-shell interface equal to R and the in-plane electron velocity v_e related to E_k by $v_e = \sqrt{4E_k/(3m_e)}$.

The PL intensity is calculated by averaging over all the contributions from the NW ensemble. For that, we obtain the distributions of the shell thickness for the investigated ensembles from SEM analysis of about 100 NWs and fit it with a Gamma probability distribution function $\Gamma(L)$ [see insets to Figs. 4(b) and 4(c)]. The PL decay is then obtained as [43]

$$I(t) = \int_0^{\infty} \Gamma(L) \exp(-t/\tau_d) dL. \quad (2)$$

$I(t)$ is fitted to the experimental data by adjusting τ_r , V , and E_k . In Figs. 4(b) and 4(c), we show fitting results for the TRPL traces measured at 5 K for the two samples with the widest shells. The agreement with the experimental data is very good and, clearly, our modeling reproduces the nonexponential character of the measured PL decays. The fitted recombination times are $\tau_r = 320 \pm 30$ ps and $\tau_r = 360 \pm 30$ ps, for the $L = 12$ nm and $L = 16$ nm samples, respectively. These values are identical within experimental error confirming *a posteriori* our assumption that τ_r is independent of the shell thickness L . A value of $\tau_r \simeq 340$ ps is by about a factor of 3 longer than the value reported for ZnTe epilayers [46,47], demonstrating the high quality of our samples. Importantly, τ_r is much longer than the average tunneling time evaluated with the fitted parameters for the mean shell thickness: $\tau_t = 12 \pm 1$ ps and $\tau_t = 31 \pm 3$ ps, for the $L = 12$ nm and $L = 16$ nm samples, respectively. This shows that carrier tunneling from the core out to the surface states is the process limiting the recombination time at low temperatures.

The fitted values of V for the $L = 12$ nm and $L = 16$ nm samples are, respectively, 148.5 meV and 150.0 meV. These values should be compared with ZnTe- $\text{Zn}_{1-x}\text{Mg}_x\text{Te}$ core-shell conduction band offsets calculated including strain. Following the model used to evaluate the strain-induced NW band gap variations [33], and taking the ratio between the conduction and valence band deformation potentials $a_c/a_v \simeq 2$ [48,49], we obtain 137 meV and 144 meV, for the $L = 12$ nm and $L = 16$ nm samples, respectively. This is a rather good

agreement given the fluctuations of the Mg concentration in the shell and uncertainty in the precise value of a_c . The fitted kinetic energies are 119 meV and 130 meV, respectively. These values are comparable to the average initial kinetic energies the electrons possess at the moment of photoexcitation: $E_k^0 = \frac{E_L - E_g}{1 + m_e^*/m_h^*}$, where E_L is the excitation energy, E_g is the band gap, and $m_{e,h}^*$ are effective masses of electrons and heavy holes [50]. $E_k^0 = 131$ meV and 142 meV, respectively. Such large values of the fitted E_k suggest that a significant fraction of electrons tunnels out of the core before cooling down to the lattice temperature. Below, we provide further arguments in favor of this conclusion. The small difference between V and E_k suggest that a thermal escape of electrons should also be present, as evidenced by the low activation energy process revealed by temperature-dependent PL measurements in Fig. 3(b).

Relying on the above analysis, we predict that the PL decay dynamics from the ensemble of NWs should exhibit a strong dependence on the excitation energy E_L . Since decreasing E_L results in lowering of E_k , one should expect a significant slowing down of the tunneling and, as a consequence, increase of the PL lifetime. In particular, for $E_k < 130$ meV and $L = 16$ nm, the tunneling times should become longer than the recombination time, leading to a suppression of the influence of the tunneling on the PL dynamics and providing access to the average recombination time only. Our modeling predicts an even more dramatic acceleration of the PL decay when increasing E_L . For $L = 16$ nm and $E_k = 149$ meV, the PL decay time becomes shorter than our temporal resolution.

The procedure described above allows us to extract the recombination times from the ensemble PL decays as a function of temperature by fitting of Eq. (2) to the data from Fig. 3(a). Fitted τ_r significantly decreases with increasing temperature as shown in Fig. 3(c). As noted above, this is due to an activation of nonradiative recombination. In Fig. 3(c), we plot the temperature dependence of τ_r evaluated from the fits together with a calculated recombination time, where we include the thermal activation of the phonon-assisted nonradiative recombination. We take $\tau_r^{-1} = \tau_{\text{rad}}^{-1} + \tau_{\text{nr}}^{-1}$, where $\tau_{\text{nr}} = \tau_{n0} \exp(E_2/(k_B T))$, with E_2 obtained previously from cw studies [see Fig. 3(b)]. The agreement between the computed curve and the extracted τ_r is very good, which confirms the assignment of the phonon-activated process as the dominant nonradiative recombination mechanism. This agreement also provides a consistency check for the whole analysis of the ensemble PL data.

IV. SINGLE NANOWIRE PHOTOLUMINESCENCE

In order to support the conclusions presented above and to gain further insight into the dynamics of carriers and excitons in ZnTe NWs, we study the PL dynamics of a single NW from the S2 sample. The excitation fluence is the same as in the measurements on the ensembles of NWs discussed above. Transient PL spectra integrated in 10-ps windows are presented in Fig. 5(a). The abrupt step at 2420 meV is the absorption of the edge-pass filter. Within 30 ps after photoexcitation, the PL spectrum is broad with full width half maximum (FWHM) ≈ 40 meV. Remarkably, the PL emission band extends from

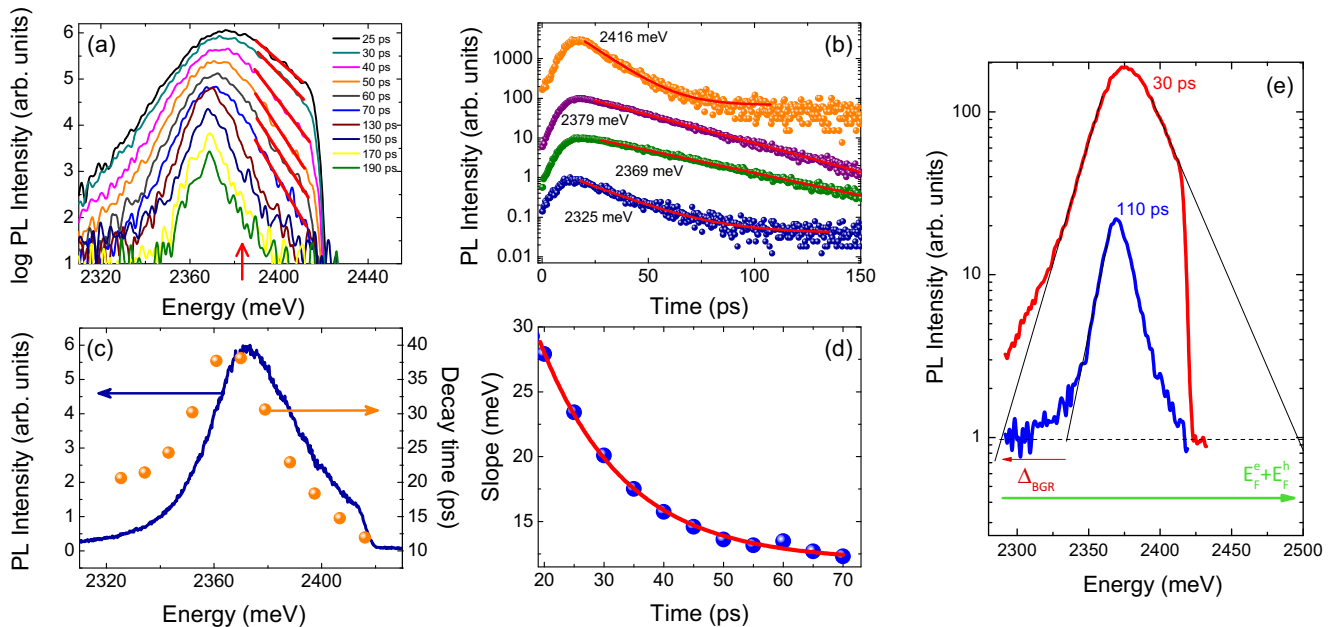


FIG. 5. (a) Transient single NW PL intensity integrated in 10-ps windows. The arrow marks the NW band gap. For better visibility, the spectra were smoothed with a fast Fourier transform filter. Red thick lines denote fitted high energy slope (see text for details). (b) (Points) Single NW PL decay traces for different photon energies. (Lines) Corresponding monoexponential fits. Scattered points at long delays are due to background noise. (c) The photon energy dependence of the PL decay times (points) superimposed on a time-integrated PL spectrum (line). (d) (Points) Fitted slope of the high energy part of the PL spectrum as a function of the time delay after photoexcitation. (Line) A monoexponential fit with a decay time of 14 ps. (e) Evaluation of the BGR. Thick lines denote transient PL spectra for 30 ps (red) and 110 ps (blue) time delays. Dashed line, background level. Thin black lines allow one to evaluate the band-gap shift due to BGR (Δ_{BGR}) and the sum of quasi Fermi levels ($E_F^e + E_F^h$). See text for details.

about 2300 meV to about 2500 meV, well above the strained NW band gap at 2382 meV, marked by an arrow in Fig. 5(a). With increasing time delay, the PL spectrum narrows, redshifts, and its high energy slope decreases. After about 150 ps after excitation, the spectrum collapses into a single peak at 2369 meV with a FWHM ≈ 20 meV. Figure 5(b) presents PL decays at different photon energies. All time traces are monoexponential. Clearly, the high and low-energy PL wings decay faster than the main peak. This is confirmed in Fig. 5(c) where we plot the fitted decay times as a function of the photon energy superimposed on the time-integrated PL spectrum. Notably, the decay times for the high- and low-energy PL wings are similar and equal to 10–20 ps.

Transient spectra presented in Fig. 5(a) allow us to trace the PL evolution from an early stage with a very high carrier density to low densities at large time delays. Since the excitation pulse has a duration of only 300 fs, the initial carrier density can be higher than the Mott density of $\sim 10^{17}$ cm $^{-3}$ resulting in the presence of a degenerate electron-hole plasma (EHP). Such large carrier densities lead to screening of the Coulomb interaction resulting in lowering of the exciton binding energy and, eventually, their disappearance. Simultaneously, exchange interaction and electron-hole correlation result in band gap renormalization (BGR)—carrier-density-dependent redshift of the energy gap [51,52]. Observation of a broad PL band at early delays was previously observed for InP and GaAs NWs and interpreted as EHP recombination accompanied by renormalization of the band gap [17,53]. In the degenerate case, the low-energy edge of the PL spectrum marks the relative energy of the renormalized gap, while the high-energy edge results from the sum of electron and hole quasi-Fermi levels. With increasing time delay, carrier density decreases and, consequently, the excitons are established.

The results presented in Fig. 5(a) reveal that at early delays the exciton resonance is smeared out consistent with the recombination from an EHP. A well-resolved exciton peak at 2369 meV appears after a delay of about 100 ps. Nevertheless, this peak coexists with the high- and low-energy wings demonstrating that the excitons coexist with free electron-hole pairs. Notably, the exciton peak energy does not shift as the screening and BGR practically compensate each other as predicted by theory [54].

The discussion above allows us to interpret the high- and low-energy PL wings as recombination of free electrons and holes and determine the carrier lifetime. As seen in Fig. 5(c), the decay time of the high energy wing is about twice shorter than decay at low energy. This is due to carrier cooling, which results in a decreasing slope of the high energy part of the EHP spectrum. Therefore, we evaluate the carrier lifetime from the low-energy PL wing and obtain a value of about 20 ps. The cooling dynamics can be obtained from the analysis of the temporal dependence of the high-energy slope. This slope is related to carrier temperature since the EHP spectrum $I(E) \propto \rho_{eh}(E)f_e(E)f_h(E)$, where $\rho_{eh}(E)$ is the joint electron-hole density of states and $f_{e,h}$ are Fermi distribution functions for electrons and holes. For quasi-2D quantum wells, where $\rho_{eh}(E)$ is a constant, $I(E) \propto \exp(-(E - E_g)/(k_B T_c))$, where E_g is the band gap energy. Thus, the high energy slope gives an estimate of the carrier temperature T_c , which is within 50% of the value obtained using more complex lineshape

models [55]. In the present case of bulklike NWs, the situation is more complicated since $\rho_{eh}(E)$ is not constant. Simple models of EHP utilize an energy-dependent prefactor and $I(E) \propto (E - E_g)^\alpha \exp(-(E - E_g)/(k_B T_c))$ with α between 1 and 2. Since precise determination of carrier temperature is beyond the scope of this work, we analyze only the slope E_s , i.e., we fit the high-energy part of the PL spectrum with $I(E) \propto \exp(-E/E_s)$ and determine the cooling time from E_s temporal dependence. The result is presented in Fig. 5(d), where E_s is plotted as a function of time delay together with a monoexponential fit. In this way, we obtain the cooling time of about 14 ps. The observed cooling dynamics are almost identical to those reported for ZnTe epilayers [46].

The obtained carrier lifetime comprises contributions from electron-hole recombination, exciton formation (at longer delays, below the Mott transition), cooling, and electron tunneling. Since the single NW measurements were performed on the S2 sample, we cannot directly compare these results to the ensemble analysis presented in Fig. 4. However, the PL dynamics of the ensemble of NW from the S2 sample [Fig. 4(a)] resembles the PL dynamics of the $L = 12$ nm sample [shown in Fig. 4(b)]. Since, as argued above, the tunneling through the shell controls the decay dynamics, we infer that the tunneling times in the S2 sample are similar to the $L = 12$ nm sample. Since the excitation powers used for both measurements are the same, this allows us to assume that the evaluated carrier lifetimes from the single NW spectroscopy are comparable to those in the sample with $L = 12$ nm. Taking the distribution shown in the inset to Fig. 4(b), we evaluate the corresponding tunneling times for three values of L from this ensemble. For narrowest shells with $L = 7$ nm, we obtain $\tau_t = 0.6$ ps, for average $L = 12$ nm, $\tau_t = 12$ ps, and for the widest $L = 17$ nm, $\tau_t = 245$ ps. These values compared with the carrier lifetime and cooling time evaluated from Fig. 5(c) show that the electron tunneling from more than half of the NWs in this ensemble occurs *before* the carriers cool down or decay either radiatively or by exciton formation. This conclusion is consistent with the fitting presented in Fig. 4, where relatively high values of electron kinetic energies were obtained.

The analysis of the single NW PL shown in Fig. 5 allows one to evaluate the exciton lifetime by fitting the decay at the exciton energy of 2369 meV—see Figs. 5(b) and 5(c). We obtain a value of about 40 ps, which is an order of magnitude shorter than the recombination time obtained from fitting of the ensemble data in Fig. 4. This is due to the fact that electron tunneling takes place also from the exciton state, where the Coulomb attraction increases the tunneling barrier by the exciton binding energy of 13 meV [56]. Therefore, we interpret the fitted value of V as an effective barrier height comprising both the conduction band offset of about 140 meV and the exciton binding energy.

In order to obtain reliable information on carrier density and the resulting band gap shrinkage due to BGR, an analysis of the entire PL spectrum is required [54,55], in particular taking into account the plasma temperature [57]. These issues are beyond the scope of this work, so here we employ a simplified approach applied to studies of BGR on single NWs [17,53]. For a delay of 30 ps, we determine the band gap shift from the low-energy wing of the PL spectrum comparing it to the lower

edge of the exciton emission line seen at a delay of 110 ps, when the excitons are clearly stable and negligible free carrier PL is observed—see Fig. 5(e). We find a BGR induced shift $\Delta_{\text{BGR}} \approx 45$ meV—see the left pointing arrow in Fig. 5(e). To estimate a carrier density n which would lead to BGR of such a magnitude, we use an expression for BGR given by Vashishta and Kalia [51]: $\Delta_{\text{BGR}} = (-4.8316 - 5.0879r_s)/(0.0152 + 3.0426r_s + r_s^2)E_B$, where $r_s^3 = 4/3\pi a_B^3 n$, and $a_B = 5.6$ nm and $E_B = 13$ meV are the bulk ZnTe exciton Bohr radius [34] and exciton binding energy [56], respectively. We find $n \approx 5.5 \times 10^{18}$ cm⁻³. The corresponding sum of zero-temperature quasi-Fermi levels for electrons and holes is 230 meV. This value agrees very well with the total extent of the PL spectrum as extrapolated beyond the filter edge—see the right pointing arrow in Fig. 5(e). Therefore, we conclude that the BGR and the quasi-Fermi levels are consistent with the evaluated electron-hole density 30 ps after photoexcitation. It is seen in Fig. 5(a) that as the time delay increases, both the low-energy PL wing, i.e., the BGR shift and the total width of the PL spectrum, i.e., the quasi-Fermi energies decrease due to decreasing density of free carriers. This analysis shows that shortly after photoexcitation the carrier gas in the NW is indeed in the degenerate limit, above the Mott transition.

V. CONCLUSIONS

In summary, we have studied the PL dynamics of ensembles and single core-shell ZnTe-Zn_{1-x}Mg_xTe NWs. Our results

show that tunneling of electrons out of the core controls the PL decay time. Thus, the growth of thicker shells result in higher PL intensities and longer PL lifetimes. Our modeling of the ensemble PL decay, based on the data from SEM analysis, allows us to extract the exciton recombination time. We find that low-temperature recombination time is about 300 ps, roughly a factor of 3 longer than reported previously for epilayers. Its temperature dependence reveals that nonradiative recombination processes are LO-phonon assisted. Comparison of the ensemble PL dynamics with studies of individual NWs shows that early after photoexcitation the presence of an electron-hole plasma leads to band gap renormalization. We find that most of the electrons tunnel out before they cool down or bind into excitons. Analysis of the spectral dependence of the decay dynamics allows one to evaluate the carrier lifetime of about 20 ps—a value limited by electron tunneling and containing contributions from electron-hole recombination and exciton formation.

ACKNOWLEDGMENTS

We thank M. Zieliński for fruitful discussions. This work partially supported by Polish National Science Centre Grants No. DEC-2011/01/D/ST5/05039 and No. DEC-2014/14/M/ST3/00484, by ANR JCJC project milliPICS and by the Region Midi-Pyrénées under Contract No. MESR 13053031. M.S. acknowledges support from the NEXT program.

-
- [1] M. H. Huang, S. Mao, H. Feick, H. Yan, Y. Wu, H. Kind, E. Weber, R. Russo, and P. Yang, *Science* **292**, 1897 (2001).
- [2] X. Duan, Y. Huang, R. Agarwal, and C. M. Lieber, *Nature* (London) **421**, 241 (2003).
- [3] F. Qian, S. Gradečak, Y. Li, C.-Y. Wen, and C. M. Lieber, *Nano Lett.* **5**, 2287 (2005).
- [4] E. D. Minot, F. Kelkensberg, M. van Kouwen, J. A. van Dam, L. P. Kouwenhoven, V. Zwiller, M. T. Borgström, O. Wunnicke, M. A. Verheijen, and E. P. A. M. Bakkers, *Nano Lett.* **7**, 367 (2007).
- [5] C. P. T. Svensson, T. Mårtensson, J. Trägårdh, C. Larsson, M. Rask, D. Hessman, L. Samuelson, and J. Ohlsson, *Nanotechnology* **19**, 305201 (2008).
- [6] Y. Huang, X. Duan, and C. M. Lieber, *Small* **1**, 142 (2005).
- [7] A. Tribu, G. Sallen, T. Aichele, R. Andre, J.-P. Poizat, C. Bougerol, S. Tatarenko, and K. Kheng, *Nano Lett.* **8**, 4326 (2008).
- [8] M. E. Reimer, G. Bulgarini, N. Akopian, M. Hocevar, M. B. Bavinck, M. A. Verheijen, E. P. Bakkers, L. P. Kouwenhoven, and V. Zwiller, *Nat. Commun.* **3**, 737 (2012).
- [9] T. Huber, A. Predojevic, M. Khoshnegar, D. Dalacu, P. J. Poole, H. Majedi, and G. Weihs, *Nano Lett.* **14**, 7107 (2014).
- [10] M. A. M. Versteegh, M. E. Reimer, K. D. Jons, D. Dalacu, P. J. Poole, A. Gulinatti, A. Giudice, and V. Zwiller, *Nat. Commun.* **5**, 5298 (2014).
- [11] J. Wang, M. S. Gudiksen, X. Duan, Y. Cui, and C. M. Lieber, *Science* **293**, 1455 (2001).
- [12] M. P. van Kouwen, M. H. M. van Weert, M. E. Reimer, N. Akopian, U. Perinetti, R. E. Algra, E. P. A. M. Bakkers, L. P. Kouwenhoven, and V. Zwiller, *Appl. Phys. Lett.* **97**, 113108 (2010).
- [13] A. de Luna Bugallo, M. Tchernycheva, G. Jacopin, L. Rigutti, F. H. Julien, S.-T. Chou, Y.-T. Lin, P.-H. Tseng, and L.-W. Tu, *Nanotechnology* **21**, 315201 (2010).
- [14] F. Patolsky and C. M. Lieber, *Mater. Today* **8**, 20 (2005).
- [15] W. U. Huynh, J. J. Dittmer, and A. P. Alivisatos, *Science* **295**, 2425 (2002).
- [16] J. Wallentin, N. Anttu, D. Asoli, M. Huffman, I. Aberg, M. H. Magnusson, G. Siefer, P. Fuss-Kailuweit, F. Dimroth, B. Witzigmann, H. Q. Xu, L. Samuelson, K. Deppert, and M. T. Borgström, *Science* **339**, 1057 (2013).
- [17] S. Perera, M. A. Fickenscher, H. E. Jackson, L. M. Smith, J. M. Yarrison-Rice, H. J. Joyce, Q. Gao, H. H. Tan, C. Jagadish, X. Zhang, and J. Zou, *Appl. Phys. Lett.* **93**, 053110 (2008).
- [18] O. Demichel, M. Heiss, J. Bleuse, H. Mariette, and A. Fontcuberta i Morral, *Appl. Phys. Lett.* **97**, 201907 (2010).
- [19] C.-C. Chang, C.-Y. Chi, M. Yao, N. Huang, C.-C. Chen, J. Theiss, A. W. Bushmaker, S. LaLumondiere, T.-W. Yeh, M. L. Povinelli, C. Zhou, P. D. Dapkus, and S. B. Cronin, *Nano Lett.* **12**, 4484 (2012).
- [20] J. O. D. Couto, D. Sercombe, J. Puebla, L. Otubo, I. J. Luxmoore, M. Sich, T. J. Elliott, E. A. Chekhovich, L. R. Wilson, M. S. Skolnick, H. Y. Liu, and A. I. Tartakovskii, *Nano Lett.* **12**, 5269 (2012).
- [21] N. Jiang, Q. Gao, P. Parkinson, J. Wong-Leung, S. Mokkalati, S. Breuer, H. H. Tan, C. L. Zheng, J. Etheridge, and C. Jagadish, *Nano Lett.* **13**, 5135 (2013).

- [22] P. Wojnar, M. Szymura, W. Zaleszczyk, L. Kłopotowski, E. Janik, M. Wiater, L. T. Baczewski, S. Kret, G. Karczewski, J. Kossut, and T. Wojtowicz, *Nanotechnology* **24**, 365201 (2013).
- [23] J. L. Boland, S. Conesa-Boj, P. Parkinson, G. Tutuncuoglu, F. Matteini, D. Ruffer, A. Casadei, F. Amaduzzi, F. Jabeen, C. L. Davies, H. J. Joyce, L. M. Herz, A. F. i Morral, and M. B. Johnston, *Nano Lett.* **15**, 1336 (2015).
- [24] Y. L. Cao, Z. T. Liu, L. M. Chen, Y. B. Tang, L. B. Luo, J. S. Jie, W. J. Zhang, S. T. Lee, and C. S. Lee, *Opt. Express* **19**, 6100 (2011).
- [25] Z. Liu, G. Chen, B. Liang, G. Yu, H. Huang, D. Chen, and G. Shen, *Opt. Express* **21**, 7799 (2013).
- [26] E. Janik, E. Dynowska, P. Dłuzewski, S. Kret, A. Presz, W. Zaleszczyk, W. Szuszkiewicz, J. F. Morhange, A. Petrouchik, S. Mackowski, and T. Wojtowicz, *Nanotechnology* **19**, 365606 (2008).
- [27] A. Artioli, P. Rueda-Fonseca, P. Stepanov, E. Bellet-Amalric, M. Den Hertog, C. Bougerol, Y. Genuist, F. Donatini, R. Andre, G. Nogues, K. Kheng, S. Tatarenko, D. Ferrand, and J. Cibert, *Appl. Phys. Lett.* **103**, 222106 (2013).
- [28] P. Wojnar, E. Janik, L. T. Baczewski, S. Kret, G. Karczewski, T. Wojtowicz, M. Goryca, T. Kazimierzczuk, and P. Kossacki, *Appl. Phys. Lett.* **99**, 113109 (2011).
- [29] P. Wojnar, E. Janik, L. T. Baczewski, S. Kret, E. Dynowska, T. Wojciechowski, J. Suffczynski, J. Papierska, P. Kossacki, G. Karczewski, J. Kossut, and T. Wojtowicz, *Nano Lett.* **12**, 3404 (2012).
- [30] M. Szymura, P. Wojnar, L. Kłopotowski, J. Suffczynski, M. Goryca, T. Smolenski, P. Kossacki, W. Zaleszczyk, T. Wojciechowski, G. Karczewski, T. Wojtowicz, and J. Kossut, *Nano Lett.* **15**, 1972 (2015).
- [31] K. Galkowski, P. Wojnar, E. Janik, J. Papierska, K. Sawicki, P. Kossacki, and J. Suffczynski, *J. Appl. Phys.* **118**, 095704 (2015).
- [32] R. S. Wagner and W. C. Ellis, *Appl. Phys. Lett.* **4**, 89 (1964).
- [33] P. Wojnar, M. Zielinski, E. Janik, W. Zaleszczyk, T. Wojciechowski, R. Wojnar, M. Szymura, L. Kłopotowski, L. T. Baczewski, A. Pietruchik, M. Wiater, S. Kret, G. Karczewski, T. Wojtowicz, and J. Kossut, *Appl. Phys. Lett.* **104**, 163111 (2014).
- [34] B. Segall and D. T. F. Marple, in *Physics and Chemistry of II–VI Compounds*, edited by M. Aven and J. S. Prener (North Holland, Amsterdam, 1967).
- [35] J. Noborisaka, J. Motohisa, S. Hara, and T. Fukui, *Appl. Phys. Lett.* **87**, 093109 (2005).
- [36] N. Sköld, L. S. Karlsson, M. W. Larsson, M.-E. Pistol, W. Seifert, J. Tragardh, and L. Samuelson, *Nano Lett.* **5**, 1943 (2005).
- [37] H. Venghaus and P. J. Dean, *Phys. Rev. B* **21**, 1596 (1980).
- [38] M. H. M. van Weert, O. Wunnicke, A. L. Roest, T. J. Eijkemans, A. Yu Silov, J. E. M. Haverkort, G. W. Hoofdt, and E. P. A. M. Bakkers, *Appl. Phys. Lett.* **88**, 043109 (2006).
- [39] E. Yablonovitch, C. J. Sandroff, R. Bhat, and T. Gmitter, *Appl. Phys. Lett.* **51**, 439 (1987).
- [40] S. Reitzenstein, S. Munch, C. Hofmann, A. Forchel, S. Crankshaw, L. C. Chuang, M. Moewe, and C. Chang-Hasnain, *Appl. Phys. Lett.* **91**, 091103 (2007).
- [41] N. Chauvin, M. H. Hadj Alouane, R. Anufriev, H. Khmissi, K. Naji, G. Patriarche, C. Bru-Chevallier, and M. Gendry, *Appl. Phys. Lett.* **100**, 011906 (2012).
- [42] S. Munch, S. Reitzenstein, M. Borgstrom, C. Thelander, L. Samuelson, L. Worschech, and A. Forchel, *Nanotechnology* **21**, 105711 (2010).
- [43] A. Gorgis, T. Fliissikowski, O. Brandt, C. Cheze, L. Geelhaar, H. Riechert, and H. T. Grahn, *Phys. Rev. B* **86**, 041302 (2012).
- [44] S.-H. Wei and A. Zunger, *Appl. Phys. Lett.* **72**, 2011 (1998).
- [45] J. H. Chang, H. M. Wang, M. W. Cho, H. Makino, H. Hanada, T. Yao, K. Shim, and H. Rabitz, *J. Vac. Sci. Technol. B* **18**, 1530 (2000).
- [46] M. J. McNamee, R. A. Taylor, P. A. Snow, W. Hayes, D. E. Ashenford, and B. Lunn, *Semicond. Sci. Technol.* **9**, 759 (1994).
- [47] F. A. Majumder, H. Kalt, C. Klingshirn, H. Stanzl, and W. Gebhardt, *Phys. Status Solidi B* **188**, 191 (1995).
- [48] D. L. Camphausen, G. A. N. Connell, and W. Paul, *Phys. Rev. Lett.* **26**, 184 (1971).
- [49] H. Mathieu, J. Allegre, A. Chatt, P. Lefebvre, and J. P. Faurie, *Phys. Rev. B* **38**, 7740 (1988).
- [50] We evaluate E_k^0 by considering parabolic and spherically symmetric conduction and valence bands. We only take into account the heavy hole band since the oscillator strength for the light hole transition is by a factor of 3 smaller.
- [51] P. Vashishta and R. K. Kalia, *Phys. Rev. B* **25**, 6492 (1982).
- [52] R. Zimmermann, *Phys. Status Solidi B* **146**, 371 (1988).
- [53] L. V. Titova, T. B. Hoang, J. M. Yarrison-Rice, H. E. Jackson, Y. Kim, H. J. Joyce, Q. Gao, H. H. Tan, C. Jagadish, X. Zhang, J. Zou, and L. M. Smith, *Nano Lett.* **7**, 3383 (2007).
- [54] H. Haug and S. Schmitt-Rink, *Prog. Quantum Electron.* **9**, 3 (1984).
- [55] J. H. Collet, W. W. Ruhle, M. Pugno, K. Leo, and A. Million, *Phys. Rev. B* **40**, 12296 (1989).
- [56] J. Camacho, A. Cantarero, I. Hernandez-Calderon, and L. Gonzalez, *J. Appl. Phys.* **92**, 6014 (2002).
- [57] M. Capizzi, S. Modesti, A. Frova, J. L. Staehli, M. Guzzi, and R. A. Logan, *Phys. Rev. B* **29**, 2028 (1984).